Surface Inductance of Superconductive Striplines

Tahereh Jabbari, *Graduate Student Member, IEEE*, and Eby G. Friedman, *Fellow, IEEE*

***Abstract*—Inductance in superconductive circuits plays a significant role in rapid single flux quantum (RSFQ) systems. Inductance estimation is a challenging issue. The microwave behavior of these inductances is characterized by the surface inductance of a line. A methodology to accurately estimate the surface inductance of a stripline is the focus of this brief. A closed-form expression describing the dependence of the surface inductance of a stripline on the line thickness, magnetic field, and current density is provided. The effects of process parameter variations on the surface inductance are also discussed. An expression to model the effects of the trapezoidal geometry of a stripline is presented. The dependence of the surface inductance on the oxide and metal layer thicknesses is also presented. The objective is to provide an accurate estimate of the surface inductance for use in automated routing of VLSI complexity RSFQ circuits.**

***Index Terms*—Single flux quantum, electronic design automation, automated layout and routing, superconductive integrated circuits.**

I. Introduction

RECENT advances in fabrication technology and electronic design automation (EDA) have enabled the increasing integration of rapid single flux quantum (RSFQ) circuits exceeding 4.2×10^6 Josephson junctions (JJs) per cm^2 with a minimum feature size of 350 nm [1]–[3]. Recent research in superconductive technology supports the development of SFQ-based EDA tools to enable the automated design of complex rapid single flux quantum circuits [4]–[12]. The reduction in feature size enhances circuit densities, but introduces design challenges. Closely spaced striplines in VLSI complexity RSFQ circuits increase coupling noise between the lines [13]. An accurate estimate of the inductances and coupling noise between different geometric structures is therefore desirable to support the development of advanced superconductive systems.

One of the primary requirements for SFQ-based automated routing is an accurate impedance model of the striplines [3], [14]. Electromagnetic simulators such as Sonnet [15] provide an accurate estimate of the impedance which depends upon certain material parameters such as the surface inductance L_s of the superconductive material. Sonnet uses this parameter L_s to model the effects of the metal thickness. Maxwell's equations are applied to determine the impedance characteristics of planar superconductive striplines [15], [16] by dividing the metal surfaces into small subsections. The magnetic field around these metal lines is incorporated into the surface inductance. The surface inductance parameter includes the boundary conditions for the magnetic fields outside the metal line.

The surface inductance plays a significant role in characterizing the impedance of a stripline within large scale integrated SFQ systems. The surface inductance is dependent upon the structure of the striplines, distance to the ground layers, thickness of the stripline, magnetic field around the lines, and current distribution inside the line. A different magnetic field distribution on each side of a stripline (symmetric and asymmetric) will produce a different current density on the lower and upper surfaces. This behavior produces different surface inductance characteristics as described by the self-inductance and the mutual inductance. Due to the imperfect nature of fabrication processes, nonuniform shapes occur in striplines [13]. This feature can change certain characteristics of the striplines such as the surface inductance. The thickness of the striplines and dielectric oxides also affect the surface inductance. Specialized guidelines and expressions are needed to provide an accurate estimate of the inductive characteristics along the surface of a stripline.

In this brief, an accurate surface inuctance expression is presented. Magnetic characterization of both symmetric and asymmetric striplines is described in Section II. The current density within the striplines and a closed-form expression for the inductance are presented in Section III. The accuracy of the expressions is also evaluated in Section III. The effects of different geometric shapes on the surface inductance are analytically described in Section IV. This brief is concluded in Section V.

II. Characteristics of Striplines

Superconductive circuits are typically composed of Josephson junctions (JJ) and thin film strips configured in several directions. In the MIT Lincoln Laboratory SFQ5ee process [3], the striplines are placed between two ground planes, which act as nearby return paths for the magnetic currents. The distance of a stripline to ground affects the surface inductance characteristics of the lines which greatly affects the design of Josephson junction-based circuits. The magnetic characteristics of the stripline are described in this section. The superconductive stripline, total current through the stripline, and magnetic field for symmetric and asymmetric striplines are described, respectively, in Sections II-A, II-B, and II-C.

A. Superconductive Stripline

The structure of a superconductive stripline is depicted in Fig. 1. The stripline with width W and thickness t is between two dielectric substrates placed above and under a ground plane. The stripline is separated from the lower and upper ground planes, respectively, by distance h and h'.

Manuscript received January 14, 2022; revised February 17, 2022; accepted March 1, 2022. Date of publication March 3, 2022; date of current version May 27, 2022. This work was supported by the Department of Defense Agency Intelligence Advanced Research Projects Activity through the U.S. Army Research Office under Contract W911NF-17-9-0001. This brief was recommended by Associate Editor C. W. Sham. *(Corresponding author: Tahereh Jabbari.)*

The authors are with the Department of Electrical and Computer Engineering, University of Rochester, Rochester, NY 14627 USA (e-mail: tjabbari@ur.rochester.edu; friedman@ece.rochester.edu).

Color versions of one or more figures in this article are available at https://doi.org/10.1109/TCSII.2022.3156533.

Digital Object Identifier 10.1109/TCSII.2022.3156533

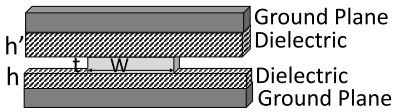

Fig. 1. Superconductive stripline between two ground layers.

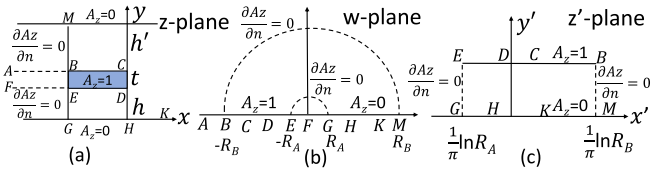

Fig. 2. Transformations of superconductive stripline [17], [18], (a) coordinates of stripline on z plane, (b) mapped structure of stripline on the w plane, and (c) mapped structure of stripline on the z' plane.

A good approximation of the magnetic field in a dielectric region can be determined from conformal mapping techniques [17], [18]. A field solution suitable for wide lines is analytically obtained from the Schwarz-Christoffel transformation [17]–[19]. Half of the stripline in the z plane (see Fig. 2(a)) is mapped into the w plane (see Fig. 2(b)) by the transformation,

$$z = f(w)$$

$$\frac{\pi z}{2h} = \alpha tanh^{-1}\sqrt{\frac{(p+q)(w+1)}{(1+q)(w+p)}} - \gamma tanh^{-1}\sqrt{\frac{w+1}{w+p}} - tanh^{-1}\sqrt{\frac{w+p}{p(w+1)}}, \quad (1)$$

where

$$\alpha = \frac{h+t+h'}{h}, \quad (2)$$

$$\gamma = \frac{h'}{h}, \quad (3)$$

$$q = \frac{1}{2}[\alpha^2 - \gamma^2 - 1 + \sqrt{(\alpha^2-\gamma^2-1)^2 - 4\gamma^2}], \quad (4)$$

$$p = \frac{q^2}{\gamma^2}. \quad (5)$$

The w plane is mapped into the z' plane (see Fig. 2(c)) by the transformation,

$$w = e^{\pi z'}. \quad (6)$$

The w plane is transformed into a region interior to and bounded by an almost parallel plate in the z' plane using a Taylor series expansion. lnR_A and lnR_B [17] shown in Fig. 2(c) are, respectively,

$$lnR_A \approx -\frac{\pi W}{2h} - 2\alpha\, tanh^{-1}\sqrt{(p+q)[p(1+q)]} + 2\gamma tanh^{-1}\frac{1}{\sqrt{p}} + ln[\frac{4p}{p-1}], \quad (7)$$

$$lnR_B \approx \gamma^{-1}[\frac{\pi W}{2h} + 2\alpha\, tanh^{-1}\sqrt{\frac{1+q}{p+q}} - 2tanh^{-1}\frac{1}{\sqrt{p}} + \gamma ln[\frac{p-1}{4}]]. \quad (8)$$

B. Current Through Stripline

The total current I in a wide stripline is obtained by applying Ampere's law to the periphery of a stripline along the z' plane. The total current of the line is

$$I = \int_{stripline} H_t \cdot dt = \frac{1}{\mu_0}\int_{stripline}\frac{A_z}{n}dt = \frac{2}{\pi\mu_0} ln\frac{R_B}{R_A} = \frac{K(w,h,t,h')}{\mu_0 h/W}, \quad (9)$$

where $K(w,h,t,\ h')$ is the fringe field factor of the stripline between two ground layers (see Fig. 1). The fringe field factor is

$$K(w,h,t,h') = \frac{h}{W}\cdot\frac{2}{\pi} ln\frac{R_B}{R_A}. \quad (10)$$

The fringe field factor of both symmetric and asymmetric striplines is dependent upon the distance between the ground layers and the stripline and the width and thickness of the striplines. A thinner stripline thickness lowers the fringe field factor (see (2), (7), (8), and (10)). A wide stripline exhibits a smaller fringe field factor as compared to a narrow stripline. Fringe field effects in narrow striplines are more significant if the width of the stripline is comparable to the dielectric thickness.

C. Distribution of Magnetic Field Around Stripline

The magnetic field in both sides of a stripline (see Fig. 2(c)) is based on the derivative of the composite functions (z and z'). An expression describing the magnetic field of a stripline is

$$\frac{\partial z'}{\partial z} = \mu_0(H_x - jH_y) = \frac{1}{\pi w}\cdot\frac{\pi(1+w)}{h(-B\sqrt{\frac{1+w}{p+w}} + \frac{A(1+q)\sqrt{\frac{(p+q)(w+1)}{(1+q)(w+p)}}}{q-w} + \frac{1}{w\sqrt{\frac{p+w}{p+pw}}})}, \quad (11)$$

where

$$B = \gamma, \quad (12)$$

$$A = \alpha\sqrt{pq}. \quad (13)$$

The magnetic field above and under the stripline is dependent on the structure of the stripline. The stripline is symmetric if $h = h'$. The magnetic field above the line is approximated by substituting $w = R_B\exp(i\theta)$ into (11) and using the first term of a Taylor series expansion. Note that R_B is much larger than 1. The magnetic field above the symmetric stripline is

$$H_x(0, h+t<y<h+t+h') \approx -\frac{1}{\mu_0 h}\cdot\frac{R_B}{R_B+k} \approx -\frac{1}{\mu_0 h}. \quad (14)$$

where $k = A\sqrt{pq} - \sqrt{p}$.

The magnetic field under the stripline is approximated by substituting $w = R_A\exp(i\theta)$ into (11) and using the first term of a Taylor series expansion. Note that R_A is much smaller than 1. The magnetic field below the symmetric stripline is

$$H_x(0, 0<y<h) \approx \frac{1}{\mu_0 h}\cdot\frac{1}{1+R_A} \approx \frac{1}{\mu_0 h}. \quad (15)$$

The magnetic field above and under a symmetric stripline is the same in magnitude but opposite in direction if the distance

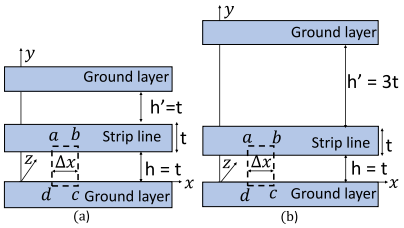

Fig. 3. Integration path of fluxoid for inductance evaluation, (a) symmetric stripline, and (b) asymmetric stripline.

between the stripline and ground layers for the two sides is the same.

For an asymmetric stripline, h' is equal to 3h in the MIT Lincoln Laboratory SFQ5ee process [3], resulting in different constants in (11). The magnetic field above the asymmetric stripline is approximated by substituting $w = R_B \exp(i\theta)$ into (11) and using the first term in a Taylor series expansion. Note again that R_B is much larger than 1. The magnetic field above an asymmetric stripline becomes

$$H_x(0, h+t<y<h+t+h') \approx -\frac{1}{\mu_0 h}\cdot\frac{R_B}{BR_B+k} \approx -\frac{1}{B\mu_0 h} \approx -\frac{1}{3\mu_0 h} \quad (16)$$

The magnetic field below an asymmetric stripline is approximated by substituting $w = R_A \exp(i\theta)$ into (11) and using the first term in a Taylor series expansion. Note again that R_A is much smaller than 1. The magnetic field below an asymmetric stripline becomes

$$H_x(0, 0<y<h) \approx \frac{1}{\mu_0 h}\cdot\frac{1}{0.9R_A+1} \approx \frac{1}{\mu_0 h}. \quad (17)$$

An asymmetric stripline exhibits an asymmetric magnetic field. The magnetic field on one side of a stripline with a distance of h = t to a ground layer is approximately three times larger than the side with a distance of h' = 3t to a ground layer. In this case, the magnetic field on each side is opposite in direction.

The x component of the magnetic field distribution is a uniform field for $|x| \leq W/2$ on each side of either a symmetric or asymmetric stripline. This magnetic field exponentially decreases [20] when x is larger than $W/2$. The y component of the magnetic field is greater near the dielectric-superconductor interface. This magnetic field penetrates the interior of the stripline within a small distance, the London penetration depth λ, decaying exponentially to zero within the stripline [20].

III. Surface Inductance of Different Striplines

The primary parameter characterizing a superconductive stripline is the surface inductance. The surface inductance provides the boundary condition for the magnetic field outside the metal, allowing the inductive characteristics and coupling noise to be estimated. An expression for the surface inductance of a stripline is presented in this section.

The inductance of a stripline is related to the ratio of the flux produced by the current flowing in the stripline to the total current flowing in the stripline. The inductance per unit length L for a stripline is evaluated by integrating path abcd of a fluxoid within the stripline (see Fig. 3). The inductance of a stripline is

$$L = \frac{1}{I}\cdot\frac{1}{\Delta z}\int_{path}(A+\mu_0\lambda^2 J)\cdot dl$$

$$= \frac{1}{I}[A_z(a)+\mu_0\lambda_1^2 J_z(a) - A_z(d) - \mu_0\lambda_2^2 J_z(d)]$$

$$= \frac{1}{I}[1+\mu_0\lambda_1^2 J_z(a) - \mu_0\lambda_2^2 J_z(d)], \quad (18)$$

where λ_1 and λ_2 are the London penetration depth of, respectively, the superconductive stripline and the ground planes. $J_z(a)$ is the current distribution inside the stripline on the bottom surface. $J_z(d)$ is the current distribution inside the ground plane on the upper surface.

The current distribution inside the striplines on both surfaces is obtained by satisfying the London equation in the superconductive region. The current distribution inside a rectangular superconductive line [19] is

$$J_z(x,y) = \nabla\times H_z = \frac{\partial H_y}{\partial x} - \frac{\partial H_x}{\partial y}, \quad (19)$$

$$J_z(x,y) = \sum_{m=0}^{\infty}\frac{b_m\zeta_m cos(\frac{m\pi y}{t})}{sinh(\zeta W)}\times[cos(\zeta x) + cosh(\zeta(W-x))] - \sum_{m=0}^{\infty}\frac{\gamma_m cos(\frac{m\pi x}{W})}{sinh(\gamma W)} \times[\alpha_{m+}cos(\gamma_m y) - \alpha_{m-}cos(\gamma_m(t-y))]. \quad (20)$$

The current density is estimated by the average magnetic field on the lower and upper surfaces of a symmetric and asymmetric stripline for $W \gg t$. In an asymmetric structure, the line exhibits a different current density on each surface of the stripline due to the asymmetric magnetic fields. The symmetric structure exhibits the same current density in both surfaces. The inductance per unit length of a stripline is determined by substituting the total current, fringe field factor, current distribution of the lower surface of the stripline, and current distribution of the upper surface of the ground layer into (18). The total inductance of a symmetric and asymmetric stripline is, respectively,

$$L_{sym} = \frac{\mu_0}{WK(w,h,t,h')}[h+\lambda_1[coth(\frac{t}{\lambda_1}) + csch(\frac{t}{\lambda_1})] + \lambda_2 coth(\frac{t}{\lambda_2})], \quad (21)$$

and

$$L_{asym} = \frac{\mu_0}{WK(w,h,t,h')}[h+\lambda_1[coth(\frac{t}{\lambda_1}) + \frac{1}{B}csch(\frac{t}{\lambda_1})] + \lambda_2 coth(\frac{t}{\lambda_2})]. \quad (22)$$

The first term of (21) and (22) represents the contribution of the external field, the second and third terms represent the contribution of the stripline, and the final term represents the contribution of the ground layer which is negligible. The difference between the inductance of a symmetric and asymmetric stripline is due to the different magnetic field and current density above the lines.

The surface inductance of a symmetric stripline is based on (21) and, for the MIT LL SFQ5ee fabrication process, is 0.1616 pH/square. This result is verified by the surface impedance technique described in [16]. An expression for the surface inductance of a symmetric line is

$$L_{s_{symm}} = \mu_0\lambda_1[coth(\tfrac{t}{\lambda_1}) + csch(\tfrac{t}{\lambda_1})]. \quad (23)$$

An expression for the surface inductance of an asymmetric line is

$$L_{s_{asymm}} = \mu_0\lambda_1[coth(\tfrac{t}{\lambda_1}) + \tfrac{1}{B}csch(\tfrac{t}{\lambda_1})]. \quad (24)$$

TABLE I
SELF-INDUCTANCE OF SUPERCONDUCTIVE STRIPLINE WITH DIFFERENT LINEWIDTHS

Striplines	Width of stripline, μm	Inductance of stripline, pH/μm, experimental [21]	Inductance of stripline, pH/μm, Sonnet	Error %	Inductance of stripline, pH/μm, 3-D inductance extractor [21]	Error %
M4-M5-M7	0.7	~ 0.39	0.41	5.12	~ 0.4	2.56
M4-M5-M7	1	~ 0.3	0.305	1.6	~ 0.31	3.33
M4-M5-M7	2	~ 0.17	0.164	3.5	~ 0.18	5.88
M4-M5-M7	4	~ 0.09	0.084	6.6	~ 0.095	5.56

TABLE II
SELF-INDUCTANCE AND MUTUAL INDUCTANCE OF DIFFERENT SUPERCONDUCTIVE STRIPLINE STRUCTURES

Striplines (coupled line, loop inductor line)	Surface inductance of striplines (24), pH/square	Inductance of loop inductor, pH, experimental [22]	Inductance of loop inductor, pH, Sonnet	Error %	Mutual inductance, pH, experimental [22]	Mutual inductance, pH, Sonnet	Error %
M4-M5-M7, M4-M6-M7	0.142, 0.166	9.3	10.3	10	1.95	1.97	1.09
M3-M4-M7, M3-M5-M7	0.158, 0.1616	13.5	14.5	7	2.75	2.82	2.67
M2-M3-M7, M2-M4-M7	0.137, 0.149	13.1	14.9	14	3.04	3.09	1.60
M1-M2-M7, M1-M3-M7	0.1365, 0.146	14.7	15.4	5	3.27	3.256	0.42
M0-M1-M7, M0-M2-M7	0.135, 0.142	15.1	15.7	3.9	3.37	3.354	0.47

The surface inductance of an asymmetric stripline is based on (22) and, for the MIT LL SFQ5ee fabrication process with $h' = 3$h, is 0.142 pH/square. The self-inductance of the asymmetric M4-M5-M7 stripline with different widths, evaluated in Sonnet by (24), is listed in Table I. These results match the experimental data within 7% [21]. The approximate self-inductance of the striplines, evaluated by a commercial 3-D inductance extractor (InductEx) [21], is also listed in Table I. These results match the experimental data within 6% [21].

The surface inductance of several structures at different distances from the stripline to the ground layers is described by (24). The surface inductance considers the effects of the thickness of the striplines and dielectrics on the self- and mutual inductance. Each structure listed in Table II exhibits two asymmetric striplines, a loop inductor and a coupled line. The self-inductance of the loop inductor, evaluated in Sonnet based on (24), is also listed in Table II. These results match the experimental data within 14% [22]. Due to differences in the physical layout, such as vias, holes in the ground planes, and port locations, an error less than 15% in the self-inductance between Sonnet and the experimental data is produced. The mutual inductance of these striplines, also evaluated in Sonnet, is listed in Table II. These results match the experimental data within 3%, less than the standard deviation of the experimental data [22]. The surface inductance expressions of (23) and (24) therefore provide an accurate estimate of the self-inductance and coupling noise between different superconductive striplines.

IV. EFFECTS OF PROCESS VARIATIONS ON INDUCTANCE

The fabrication process of the MIT Lincoln Laboratory SFQ5ee technology patterns niobium (Nb) layers with 248 nm photolithography and high density plasma etching steps [3]. It is desirable to pattern the Nb striplines with a rectangular cross section and uniform thickness. Due to resolution limitations and variations in the photolithography process, nonuniform shapes often occur in striplines. These variations greatly affect the stripline characteristics and circuit yield.

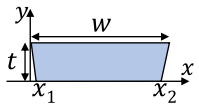

Fig. 4. Cross section of a trapezoidal stripline.

Process variations is a challenging issue in large scale integrated circuits. Parameters variations in superconductive striplines are related to the dielectric thickness h and h', metal thickness t, and metal width W. For fabricated striplines with width $W \pm \Delta W$, the equivalent cross section can be approximated by a trapezoidal shape and a different thickness [13]. The effects of a trapezoidal shape on the surface inductance are described in Section IV-A. The effects of thickness variations on the surface inductance are described in Section IV-B.

A. Trapezoidal Geometry of a Stripline

Different stripline geometries produce different boundary conditions on the magnetic field and current distribution. The different magnetic characteristics of a stripline produce a different surface inductance. The structure of a trapezoidal stripline is depicted in Fig. 4. The boundary conditions for the magnetic field across a trapezoidal stripline should satisfy the London equation in the superconductive region. These boundary conditions for a trapezoidal stripline are described by the following expressions,

$$H_x = h_x(x, 0), \quad y = 0 \text{ and } x_1 < x < x_2 \tag{25}$$

$$H_x = h_x(x, t), \quad y = t \text{ and } 0 < x < W \tag{26}$$

$$\frac{\partial H_x}{\partial x} = 0, \quad x = \frac{-x_1}{t}(y - t), \frac{w - x_2}{t}(y + \frac{tx_2}{W - x_2}) \tag{27}$$

$$H_y = h_y(\frac{-x_1}{t}(y - t), y), \quad 0 < x < x_1 \tag{28}$$

$$H_y = h_y(\frac{W - x_2}{t}(y + \frac{tx_2}{W - x_2}), y), \quad x_2 < x < W \tag{29}$$

$$\frac{\partial H_y}{\partial y} = 0. \quad y = 0, t \tag{30}$$

Considering these boundary conditions, the constants in (20) are determined by the following expressions,

$$a_{0_-} = \frac{1}{W}\int_{x_1}^{x_2} h_x(x, 0)dx, \tag{31}$$

$$a_{0_+} = \frac{1}{W}\int_{0}^{W} h_x(x, t)dx, \tag{32}$$

$$b_0 = \frac{1}{t}\int_{0}^{t} h_y(\frac{W - x_2}{t}(y + \frac{tx_2}{W - x_2}), y)dy. \tag{33}$$

For wide lines where $W \gg t$, the effects of these constants, (31) to (33), on the magnetic field and current are negligible. A wide trapezoidal geometry therefore does not affect the surface inductance, self-inductance, and mutual inductance. For narrow lines where $W \approx t$ and $W \approx \lambda$, the effects of the fringing fields can be considerable. These fringing effects decrease the reluctance of the magnetic path and therefore increase the line inductance. The effects of linewidth variations can therefore be significant in narrow lines. The surface inductance of a narrow symmetric stripline is

$$L_s = \mu_0\lambda_1[coth(\frac{t}{\lambda_1}) + csch(\frac{t}{\lambda_1}) + \frac{2b_0}{\lambda_1}exp(-\frac{W}{2\lambda_1})]. \tag{34}$$

TABLE III
DEPENDENCE OF SURFACE INDUCTANCE TERMS ON THE THICKNESS OF A STRIPLINE (IN A 10 KA/CM^2 PROCESS TECHNOLOGY)

Thickness (nm)	t/λ	coth (t/λ)	csch (t/λ)	Surface inductance
450	5	1	0.013	0.13169
360	4	1.001	0.037	0.13494
200	2.2	1.025	0.224	0.16237
135	1.5	1.105	0.470	0.20475
90	1	1.313	0.851	0.28132

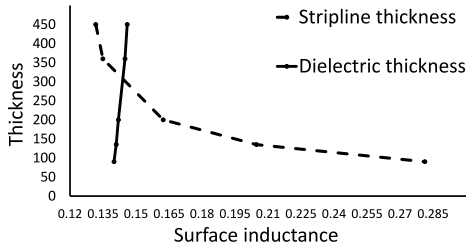

Fig. 5. Dependence of dielectric thickness (solid line) and stripline thickness (dashed line) on the surface inductance.

B. Effect of Layer Thickness on Surface Inductance

Variations in the MIT LL SFQ5ee fabrication process produce a nonuniform thickness in the metal and dielectric layers. These thickness variations affect the surface inductance, self-inductance, and mutual inductance. The effects of variations in the thickness of the dielectric and stripline are described below.

1) Thickness Variations of Oxide Dielectric: Thickness of the dielectric layers plays an important role in the surface inductance characteristics of a stripline. The thickness variations in the dielectrics change the distance of a stripline to the ground layers, affecting (11). These effects produce a different average magnetic field around the stripline and current distribution on the lower and upper surface within the stripline. The surface inductance of the striplines is dependent on these magnetic characteristics (see (11), (23), and (24)). The dependence of the surface inductance on the dielectric thickness is shown in Figure 5. A stripline with a thicker dielectric exhibits a larger inductance.

2) Thickness of the Striplines: The surface inductance and self-inductance depend upon the thickness of the striplines, as described in (21) to (24). The effects of the thickness and penetration depth λ of a stripline are modeled by the *coth* and *csch* terms in (21) to (24). These terms, for different stripline thicknesses with a 90 nm penetration depth, are listed in Table III. The dependence of the surface inductance on the stripline thickness is shown in Figure 5. The thicker lines produce a lower surface inductance and self-inductance. Thicker lines also exhibit a larger fringing field factor. Increasing the thickness of the Nb striplines decreases the self-inductance and coupling noise between layers.

V. CONCLUSION

A superconductive stripline is a primary structure in the automated routing of VLSI complexity RSFQ circuits. Accurate characterization of striplines is necessary to determine a key parameter, the surface inductance L_s. Expressions are presented in this brief that characterize the surface inductance of symmetric and asymmetric striplines. Analytic estimates of the mutual inductance and self-inductance of these striplines match experimental data within, respectively, 3% and 7%. The effects of the trapezoidal shape and layer thickness on the surface inductance are also described. Closed-form expressions are provided to accurately estimate the self- and mutual inductance of superconductive striplines.

ACKNOWLEDGMENT

The content of the information does not necessarily reflect the position or the policy of the United States Government, and no official endorsement should be inferred.

REFERENCES

[1] G. Krylov and E. G. Friedman, *Single Flux Quantum Integrated Circuit Design*. Cham, Switzerland: Springer Publ., 2022.
[2] O. A. Mukhanov, "Superconductive single-flux quantum technology," in *Proc. IEEE Int. Solid-State Circuits Conf.*, San Francisco, CA, USA, Feb. 1994, pp. 126–127.
[3] S. K. Tolpygo *et al.*, "Advanced fabrication processes for superconducting very large-scale integrated circuits," *IEEE Trans. Appl. Supercond.*, vol. 26, no. 3, pp. 1–10, Apr. 2016.
[4] J. Zhai, Y. Cai, and Q. Zhou, "Placement and routing methods considering shape constraints of JTL for RSFQ circuits," *IEEE Trans. Circuits Syst. II, Exp. Briefs*, vol. 68, no. 5, pp. 1571–1575, May 2021.
[5] G. Datta, Y. Lin, B. Zhang, and P. A. Beerel, "Metastability in superconducting single flux quantum (SFQ) logic," *IEEE Trans. Circuits Syst. I, Reg. Papers*, vol. 68, no. 5, pp. 1990–2002, May 2021.
[6] G. Pasandi, A. Shafaei, and M. Pedram, "SFQmap: A technology mapping tool for single flux quantum logic circuits," in *Proc. IEEE Int. Symp. Circuits Syst.*, Florence, Italy, May 2018, pp. 1–5.
[7] T. Jabbari and E. G. Friedman, "Global interconnects in VLSI complexity single flux quantum systems," in *Proc. Workshop Syst. Level Interconnect Problems Pathfinding Workshop*, Nov. 2020, pp. 1–7.
[8] T. Jabbari, G. Krylov, S. Whiteley, J. Kawa, and E. G. Friedman, "Repeater insertion in SFQ interconnect," *IEEE Trans. Appl. Supercond.*, vol. 30, no. 8, pp. 1–8, Dec. 2020.
[9] M. Pedram and Y. Wang, "Design automation methodology and tools for superconductive electronics," in *Proc. IEEE/ACM Int. Conf. Comput.-Aided Des.*, San Diego, CA, USA, Nov. 2018, pp. 1–6.
[10] W. Deng, J. Xu, X.-Z. Gao, and H. Zhao, "An enhanced MSIQDE algorithm with novel multiple strategies for global optimization problems," *IEEE Trans. Syst., Man, Cybern., Syst.*, vol. 52, no. 3, pp. 1578–1587, Mar. 2022.
[11] W. Deng, J. Xu, H. Zhao, and Y. Song, "A novel gate resource allocation method using improved PSO-based QEA," *IEEE Trans. Intell. Transp. Syst.*, early access, Oct. 1, 2020, doi: 10.1109/TITS.2020.3025796.
[12] W. Deng *et al.*, "Quantum differential evolution with cooperative coevolution framework and hybrid mutation strategy for large scale optimization," *Knowl. Based Syst.*, vol. 224, no. 19, pp. 1–14, Jul. 2021.
[13] J. Mao, O. Wing, and F.-Y. Chang, "Synthesis of coupled transmission lines," *IEEE Trans. Circuits Syst. I, Fundam. Theory Appl.*, vol. 44, no. 4, pp. 327–337, Apr. 1997.
[14] R. N. Das *et al.*, "Large scale cryogenic integration approach for superconducting high-performance computing," in *Proc. IEEE Electron. Compon. Technol. Conf.*, Orlando, FL, USA, Aug. 2017, pp. 675–683.
[15] "3D Planar High-Frequency Electromagnetic Software." Nov. 2020. [Online]. Available: https://www.sonnetsoftware.com/products/sonnet-suites/
[16] A. R. Kerr, "Surface impedance of superconductors and normal conductors in EM simulators," NRAO, Charlottesville, VA, USA, NRAO Electronics Division Internal Rep. 302, Jan. 1999.
[17] W. H. Chang, "Analytical IC metal-line capacitance formulas," *IEEE Trans. Microw. Theory Techn.*, vol. TMTT-24, no. 9, pp. 608–611, Sep. 1976.
[18] C. K. Koc and P. F. Ordung, "Schwarz-Christoffel transformation for the simulation of two-dimensional capacitance (VLSI circuits)," *IEEE Trans. Comput.-Aided Design Integr. Circuits Syst.*, vol. 8, no. 9, pp. 1025–1027, Sep. 1989.
[19] W. H. Chang, "The inductance of a superconducting strip transmission line," *J. Appl. Phys.*, vol. 50, pp. 8129–8134, Dec. s1979.
[20] T. V. Duzer and C. W. Turner, *Principles of Superconductive Devices and Circuits*, 2nd ed. London, U.K.: Elsevier, 1981.
[21] S. K. Tolpygo, E. B. Golden, T. J. Weir, and V. Bolkhovsky, "Inductance of superconductor integrated circuit features with sizes down to 120 nm," *Supercond. Sci. Technol.*, vol. 34, no. 8, pp. 1–24, Ju1. 2021.
[22] C. J. Fourie, C. Shawawreh, I. V. Vernik, and T. V. Filippov, "High-accuracy InductEx calibration sets for MIT-LL SFQ4ee and SFQ5ee processes," *IEEE Trans. Appl. Supercond.*, vol. 27, no. 2, pp. 1–5, Mar. 2017.